



UMS-Net++: Modified SwinTransformer for Cardiac MRI Segmentation and Classification

Shanmugasundaram Jaganathan^{1*}, Vinoth Kumar Bojan², Saravanakumar Natarajan³

¹ Department of EEE, Vivekanandha College of Engineering for Women, Tiruchengode 637205, India

² Department of EEE, Dr. Mahalingam College of Engineering and Technology, Pollachi 642003, India

³ Department of ECE, Dr. Mahalingam College of Engineering and Technology, Pollachi 642003, India

Corresponding Author Email: shanmugam.mit@gmail.com

Copyright: ©2025 The authors. This article is published by IETA and is licensed under the CC BY 4.0 license (<http://creativecommons.org/licenses/by/4.0/>).

<https://doi.org/10.18280/ts.420112>

ABSTRACT

Received: 3 August 2024

Revised: 29 September 2024

Accepted: 10 December 2024

Available online: 28 February 2025

Keywords:

cardiac disease, Magnetic Resonance Imaging (MRI), segmentation, SwinTransformer

Cardiac disease detection using Magnetic Resonance Imaging (MRI) inputs is encouraged using intelligent computer-aided visual processing techniques in smart health. The pixel-dependent segmentation and classification are automated for disease detection and diagnosis in its early stages using conventional image processing. This article introduces a Unit-Modified SwinTransformer Network (UMSN) for thwarting pixel differentiation issues in cardiac MRI analysis. The proposed network is different from the conventional SwinTransformer Network by grouping similar dimension pixels from 2×2 to 16×16 segmentation. In this grouping the analysis layer is trained using unanimous feature extractable pixels and the end-of-pixel region is the segment boundary detected. In this detection process, the coinciding pixel boundaries with similar features are used for training the fundamental segment of the consecutive boundaries. Therefore, the disparity between grouped and independent boundary segments is identified as a false rate. This identified unit is used for independent training across various labeled classifications from the training inputs. Therefore, the disparity between the boundaries or segment pixels is used for identifying flaws in the input MRI.

1. INTRODUCTION

Magnetic resonance imaging (MRI) is a medical testing method that exact structure and condition of internal organs. MRI images are commonly used for disease detection, treatment, monitoring, and diagnosis processes. MRI images-based cardiac disease detection and diagnosis processes are layered and sequential in healthcare applications [1]. A delayed-enhancement (DE) method using MRI images is used for cardiac disease detection. The DE method analyses the left ventricle (LV) and right ventricle (RV) characteristics for the diagnosis [2]. The DE method recognizes the important features and patterns from MRI images. The DE method maximizes the precision in disease detection for the diagnosis [3]. A machine learning (ML) algorithm is also employed for cardiovascular disease (CVD) detection. MRI images are used here which produce feasible information for disease detection [4]. The ML algorithm segments the data which decreases the computational complexity of the system. The exact types of CVD are also detected which provides feasible diagnosis services for the patients [5].

Image segmentation is a method that segments the images based on quantitative biomarkers and pixels. The important region of interest (ROI) is segmented using MRI images that produce relevant data for cardiac disease detection. It segments images into regions such as texture, size, level, color, brightness, contrast, and condition of the patient's heart [6]. An MRI-based segmentation method is used for the heart disease classification process. The MRI images predict the key

values that contain important features or disease detection [7]. A pixel-wise classification method is used to evaluate the volumetric features of the cardiac disease classification [8]. The exact types of the disease minimize the complexity ratio of the systems. A DE-MRI-based model is also used for the cardiac disease classification process. The DE-MRI models predict the crucial types of heart diseases of the patients [9]. The DE-MRI model also evaluates the multi-scale transformer which is presented in MRI images. The actual cause of the disease is identified which provides feasible data for further diagnosis process [10].

The actual goal of the ML algorithm is to increase the overall accuracy of the detection process. The ML algorithms are used for cardiac disease classification to enhance the efficiency in providing treatment for patients [11]. A convolutional neural network (CNN) algorithm-based cardiac disease classification method is used in healthcare centers. The CNN algorithm uses a feature extraction technique is used here to extract the features for the detection process [12]. The extracted features contain key heart structures from MRI images. Both right and left ventricle cavities and functionalities of the hearts for detection and classification processes [13]. The CNN algorithm-based method increases the accuracy of cardiac disease detection. A deep learning (DL) algorithm-based automatic segmentation method is used for the cardiac disease detection process [14]. The DL algorithm identifies the regional cardiac functions to segment the MRI images. The DL algorithm gathers the necessary information from MRI images for disease detection. The MRI images are

used here as inputs that provide exact content for the disease detection process [15]. The prime contributions are:

- Designing a UMSN for addressing the pixel differentiation problem in diagnosing cardiac diseases through MRI inputs
- Performing a dimension-based segmentation to improve the accuracy in detecting disease infections with boundary differentiation
- Performing a MATLAB-based experimental assessment and metric-based comparative assessment for the proposed validation.

2. RELATED WORKS

Li et al. [16] proposed a weighted decision map based on a convolutional neural network (CNN) framework for cardiac magnetic resonance (MR) segmentation. The proposed framework is mainly used to segment the complex issues that are presented in MR images. A map extractor is used in the framework to categorize the pixel for the segmentation. The proposed framework enhances the feasibility ratio of the image segmentation.

Xu et al. [17] developed a boundary mining with learning for myocardial infarction segmentation. A semi-supervised learning algorithm is used to classify the segments as per the condition of the patients. The semi-supervised learning algorithm analyses both spatial and temporal features which produce optimal values for the segmentation. The developed method reduces the time consumption level in the infarction segmentation.

Wang et al. [18] introduced an improved U-net model for segmentation in multi-sequence cardiac MR images. The main aim of the model is to segment the features of MRI images. The introduced model uses a selective kernel (SK) module to evaluate the features that contain data for the segmentation. The introduced model decreases the energy consumption ratio in the computation.

Su et al. [19] proposed a new two-stage deep learning (DL) model, named Res-DUNet for cardiac right ventricular (RV) segmentation. It detects the short-axis slices from the given MRI images. It also identifies the region of interest (ROI) of RV from the images. It decreases the complexity of image segmentation. The proposed Res-DUNet model increases the performance and feasibility range of segmentation.

Cui et al. [20] designed a new attention-guided U-net architecture using short-axis MRI images for cardiac segmentation. The designed model is mostly used for ventricle segmentation which detects the multi-scale features of the images. The MRI images minimize the time and energy consumption in the segmentation and computation processes. The designed model increases the accuracy of the cardiac segmentation.

Wang et al. [21] developed a multi-scale deep learning network (MMNet) for the left ventricular (LV) segmentation process. It is mainly used for LV segmentation based on cardiac MRI images. A feature extraction technique is employed to extract the features and patterns of cardiac ventricular. The developed MMNet maximizes the accuracy in LV localization and segmentation processes.

Li et al. [22] introduced a triple attention-based multi-modality (TAUNet) model for cardiac pathology segmentation. The introduced model analyses the exact relationship between modalities and attention. A fusion encoder is used here to

extract the modality features from cardiac MRI images. The TAUNet model reduces the time consumption of the cardiac pathological. The introduced model improves the performance level in cardiac pathology.

Abdelraouf et al. [23] proposed a lightweight localization based on U-Net for the segmentation process. It is a CNN-based framework to measure the features from cardiac MRI images. The CNN-based framework detects the ROI values for the ventricular segmentation. The proposed framework maximizes the accuracy and feasibility of cardiac segmentation.

Joshi et al. [24] designed a dense deep transformer model for medical image segmentation. The designed model uses a CNN algorithm to identify the features from cardiac segmentation. The optimal features and patterns of the ventricular are extracted from the images that minimize the computation cost. Experimental results show that the designed model enhances the performance range of the segmentation.

Wang et al. [25] introduced a two-stage progressive unsupervised domain adaptive network (TSP-UDANet) for cardiac segmentation. The actual goal of the model is to reduce the domain shift ratio during the segmentation process. The actual target domains are evaluated based on ROI from the given MRI images. The introduced TSP-UDANet model provides effective segmentation services for the cardiac diagnosis process.

Zou et al. [26] developed a new LV segmentation approach using tagged MRI images. Local sine-wave modeling (SinMod) identifies the key characteristics of cardiac ventricular. The identified characteristics produce feasible information for LV segmentation. It predicts the exact location of cardiac diseases and enhances the efficiency of the diagnosis process. When compared with other approaches, the developed approach enlarges the accuracy of the LV segmentation.

Chen et al. [27] proposed a multi-scale dilation convolution module-based segmentation method. The proposed method is commonly used for atrial septal defect (ASD) detection based on MRI images. The proposed method uses a k-means algorithm which evaluates the information for the segmentation. Experimental results show that the proposed method improves the overall feasibility and significance range of the segmentation process.

Zhang et al. [28] introduced an automatic segmentation based on a fully convolutional dense (FCD) network. A dilated convolution algorithm is also used for the segmentation which minimizes the latency in the computation. The introduced method uses cardiac MRI images that produce optimal data for further processes. The introduced method enhances the performance and reliability level of the network.

Hu et al. [29] proposed a fully automatic segmentation method using a deeply supervised network. The proposed method detects the both right and left large-scale cardiac for the segmentation process. It segments the heart issues based on the severity level of the patients. It also minimizes the computational complexity ratio in the right and left ventricular segmentation process. The proposed method enlarges the precision of the cardiac segmentation process.

Yan et al. [30] developed a new SegNet-based model for the LV segmentation process using MRI images. The main aim of the model is to diagnose the myocardial disease of the patients. It detects the necessary ROI from the given cardiac MRI images. The ROI eliminates the unwanted pixels during analysis and segmentation processes. The developed model

provides optimal technical support to enhance the feasibility of the segmentation.

Singh et al. [31] introduced an attention-guided residual W-Net model for the cardiac segmentation process. It uses MRI images that contain information that is relevant to both right and left ventricles. The MRI images capture the data which decreases the latency in the computation. When compared with other models, the introduced model improves the performance and significance level of the network.

Cardiac diseases are an important global health concern, and prior detection is decisive for efficacious treatment and enhanced patient results. The MRI scan has emerged as a beneficial tool for cardiac analysis due to its non-invasive nature and high-quality imaging. Suganyadevi et al. [32] have shown that to improve the precision and efficacy of cardiac disease detection, intelligent computer-aided visual processing techniques have gained preeminence in the field of smart health. One useful approach in this domain is the UMSN, which is the precise system designed to orate the problems related to pixel differentiation in cardiac MRI analysis.

3. PROPOSED UNIT-MODIFIED SWINTRANSFORMER NETWORK

UMSN is a different approach that engages a unique master plan by associating the similar-dimension pixels into segments ranging from 2×2 to 16×16 . This segmentation perspective is instrumental in enhancing the accuracy of disease detection. Within this grouped pixel analysis, an indispensable layer is trained using pixels that manifest unanimous feature extraction. This training methodology allows the framework to determine the segment boundaries efficaciously. During the boundary detection procedure, this process organizes the coinciding pixel boundaries with similar features for training the fundamental segment of consecutive boundaries. The UMSN denotes an innovative advancement in cardiac MRI observation for disease detection and diagnosis. By associating the pixels, determining the disparities, and purifying its training process, UMSN contributes importantly to the prior detection of cardiac diseases, which leads to better patient care and results in the realm of smart health. In Figure. 1 the overall process of the proposed network is portrayed.

The MRI-Cardiac inputs are taken for further feature extraction operations. From the inputs, the high-quality images contribute precise functionalities that help provide the basement for the subsequent feature extraction operations. Through the proposed advanced image processing operations, the same characteristics and frameworks are extracted for future procedures. These extorted characteristics are necessary for the precise determination of cardiac diseases, which helps detect the diseases in their earlier stages. MRI-Cardiac inputs help in the precise analysis and then the detection of heart-based diseases, producing indispensable insights into the patient's health. The process of analyzing the MRI-Cardiac inputs for further operation is explained in the upcoming equation:

$$\left. \begin{aligned} \gamma_a &= a - 2^n \\ \text{if } \frac{2^n}{a} &\in N \\ a - 2^n &\geq 0 \\ \hat{\gamma} &= N - \gamma^{n-1} \\ \gamma' &= \hat{\gamma} + \frac{N}{2}(n * 2) \\ \gamma(N) &= \frac{N}{2} \left[\sum_{n=1}^N \left(\gamma * \frac{n}{2} \right) \right] \\ \gamma_n &= \gamma_a + \frac{N}{2}(n * \gamma) \end{aligned} \right\} \quad (1)$$

where, γ is denoted as the MRI-Cardiac inputs, a is represented as the analysis procedure, and N is represented as the functionalities detected from the inputs. Now the features are extracted from the given MRI-Cardiac inputs. After the determination of the MRI-Cardiac inputs, the feature extraction process is performed which helps in separating and quantifying the distinctive features within the acquired cardiac input images. Features extract the entire information of the input images which includes the textural features. This operation helps in detecting the variations in the structure. In this process, the smoothness, or the tendency of the tissues is derived for further procedures. These characteristics produce valuable insights into the cardiac tissues insane and also help detect the subtle abnormalities that assist the healthcare in diagnosing priory. The process of feature extraction from the detected MRI-Cardiac inputs is explained in the following equation given below:

$$\left. \begin{aligned} \beta &= F_a \\ F &\in \gamma^{n \times n} \\ a &= F^n \beta \\ n &\in \{0,1\}^N \\ \hat{\beta} &= N \odot \beta \\ \hat{a} &= F^n \hat{\beta} \\ a^* &= \sum_{n=1} (a) + \gamma \| \beta - n \odot (F_a)^2 \| \\ a^* &= \frac{\gamma_a}{\gamma_\beta} \\ \beta^* &= \frac{\gamma_a}{\gamma_\beta} * \frac{\gamma_{\hat{\beta}}}{\gamma_n} * \frac{\gamma_n}{\gamma_a} \end{aligned} \right\} \quad (2)$$

where, β is represented as the extraction of the characteristics, and F is denoted as the detected textural features in the acquired inputs. Now the representation of the dimension's operation is performed. This is the process of denoting the data in both the 2×2 to 16×16 dimensions. This plays an important role in cardiac MRI analysis. This operation engages the structuring of the extracted features and textural information in two distinct dimensions, producing the complete representation of the cardiac data. Therefore, in the 2×2 dimensions, the refined details and localized variations within the acquired input MRI input images are captured. This permits for the more explored assessment of the particular regions of the heart, making it fit for the detection of the irregularities within it. The dimension representation process is illustrated in Figure 2.

The input γ is used for extracting $F \forall \beta$ such that $F \leq \beta$ condition is to be satisfied. Based on the $\gamma(N) = \frac{N}{2} \forall n \in N$, the α is performed in representing the γ at its least and maximum formats. In this representation, the F is validated based on available $\gamma^{n-1} \forall N$ such that $\hat{\beta} = N \odot \beta$ is the idle condition. Therefore, for the $F \leq \beta$ satisfying condition, segmentation is pursued (Figure 2). Also, the 16×16 dimension provides an expanded perspective by integrating the data over larger cardiac image areas. This dimension is important for dehiscing the frameworks and overall cardiac structure and functionalities. By denoting the data in both dimensions, the algorithms assess the comprehensive dataset that associates the refined data with the precision and reliability of cardiac disease detection and diagnosis. This dimension representation improves the utilization of the MRI data in enhancing patient care and its outputs. The process of the dimension representation of the acquired data is explained

in the equation below:

$$\left. \begin{aligned}
 \beta(j) &= \begin{cases} \beta_\gamma(j) & \text{if } j \in N \\ \frac{\beta_\gamma(j) + N_\beta(j)}{1 + N} & \text{if } j \in N \end{cases} \\
 F_{\gamma\beta}(a, \beta, \gamma) &= F^n + \frac{\gamma}{1 + \gamma} F(N \odot \beta) \\
 &\begin{cases} 1 & \text{if } F \notin N \\ \frac{1}{1 + \gamma} & \text{if } F \in N \end{cases} \\
 \frac{\partial F_n}{\partial a_n} &= F^n a \gamma \\
 F &\in N^{n \times n} \\
 F \odot N &\approx \frac{\gamma}{\beta}
 \end{aligned} \right\} (3)$$

where, j represents the dimension representation of the data. Now the SwinTransform process takes place in this MRI analysis procedure. It is used in thwarting the pixel differentiation issued in the MRI cardiac analysis. This process is important in the MRI cardiac analysis particularly designed to address the issues that are related to pixel differentiation. It helps enhance the precision and efficaciousness of disease detection within the cardiac MRI data. In this swim transformer process, the segmentation and boundary detection procedures are performed for further procedures. The SwinTransform process is explained in the equation below:

$$\left. \begin{aligned}
 \{F_j^i\} &= \text{swirm}(I_n) \\
 n &= 1, 2, 3, 4, 5 \\
 \{F_v^i\} &= \text{swirm}(I_\gamma) \\
 \gamma &= 1, 2, 3, 4, 5 \\
 I &= I_0 * \beta \\
 I_1 &= I_2 * \beta_1 \\
 \beta_1 &= FN \\
 a_1 &= f_1(F^N(N_1 \odot \beta)) \\
 a_n &= f_n(F^N(N_n \odot \beta_n)) \\
 a_F &= a_1 + a_n \\
 \bar{a}_1 &= F(N \odot \beta) \\
 \bar{a}_n &= F_n(N_n \odot \beta)
 \end{aligned} \right\} (4)$$

where, I is denoted as the operation of SwinTransform in the further processes. Now the segmentation process is performed in the SwinTransform operation. This algorithm helps in

grouping the pixels with similar features into segments, which range from 2×2 to 16×16 in dimensions. By associating similar pixels, the operation reduces the issues and problems based on pixel differentiation. This segmentation process is useful in simplifying the difficult cardiac images, permitting an efficient focused analysis.

$$\left. \begin{aligned}
 \beta_i &= \sum_{n=1}^j (F(a_i)) a_i + a_i \\
 \hat{\beta}_i &= \sum_{n=1}^j (F(N - \gamma \odot N - n)) F - N + a_i \\
 \beta_i &= \sum_{n=1}^j (\gamma N(\hat{\beta}_i)) + \hat{\beta}_i \\
 (a, \beta) &= 1 - \frac{2}{Nj} \sum_{j=1}^j \frac{\sum_{i=1}^j a_{ij} \beta_{ij}}{\sum_{i=1}^j a_{ij}^2 + \sum_{i=1}^j \beta_{ij}^2} \\
 \sum_{n=1}^j (a, \beta) &= \frac{1}{I} \sum_{i=1}^j \sum_{j=1}^j a_{ij} \log \beta_{ij} \\
 (a, \beta) &= N(a, \beta) + N_{ij}(a, \beta)
 \end{aligned} \right\} (5)$$

$$\left. \begin{aligned}
 \varepsilon_{ij} &= \frac{2 \times |a \cap \beta|}{|a| + |\beta|} \\
 \varepsilon_{ij} &\leftarrow F_n(a_n - 1) \\
 n_n &\leftarrow \beta_1 \cdot \gamma_{n-1} + (1 - \beta_1) \\
 \gamma_n &\leftarrow \gamma_{n-1} \cdot a(\varepsilon + a\beta) \\
 \gamma_{ij} &= \frac{|a \cap \beta| + ij}{|a_{ij}| + |b_{ij}|} \\
 \gamma_n &= \frac{|a \cup \beta| * ij}{|a_{ij}| + |b_{ij}|} \\
 F_{ij} &= \frac{|a \cap \beta| + ij}{|a_{ij}| + |b_{ij}|} \\
 F_n &= \frac{|a \cup \beta| * ij}{|a_{ij}| + |b_{ij}|}
 \end{aligned} \right\} (6)$$

These steps assess the meaningful categories to segments based on their distinct features, helping differentiate between the various parts of the heart and surrounding tissues. The segmentation using a SwinTransformer is presented in Figure 3.

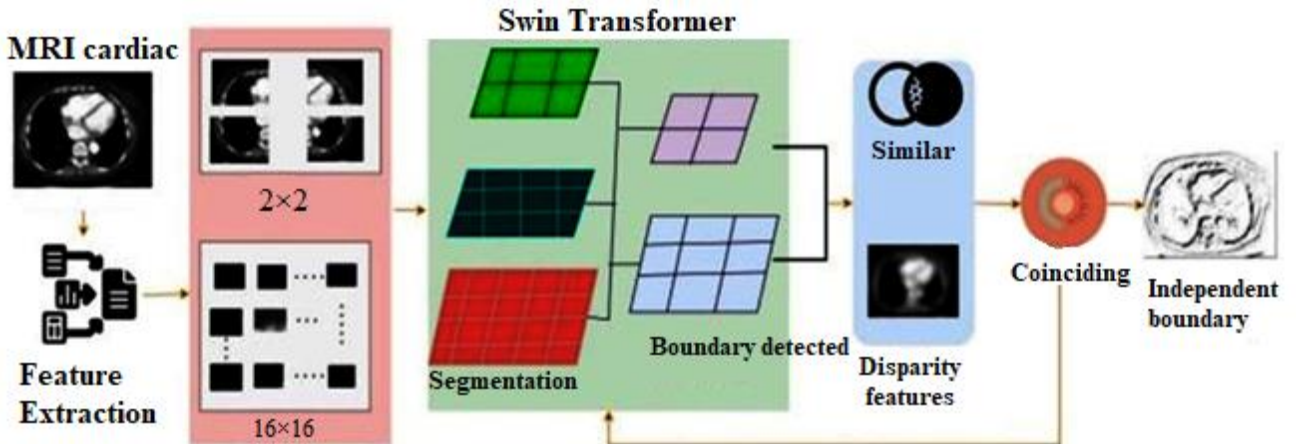


Figure 1. Overall process of the proposed network

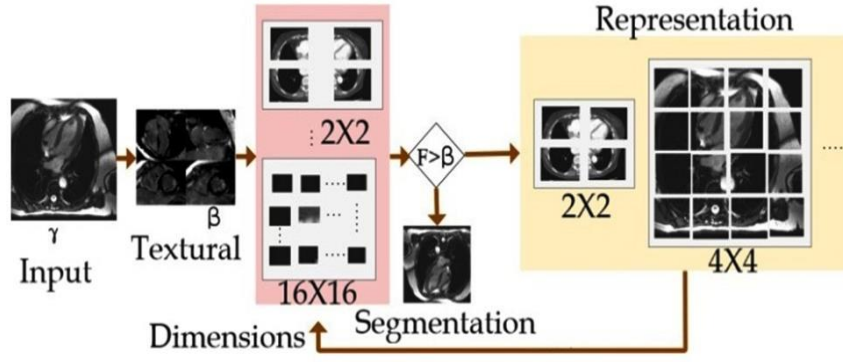


Figure 2. Dimension illustration

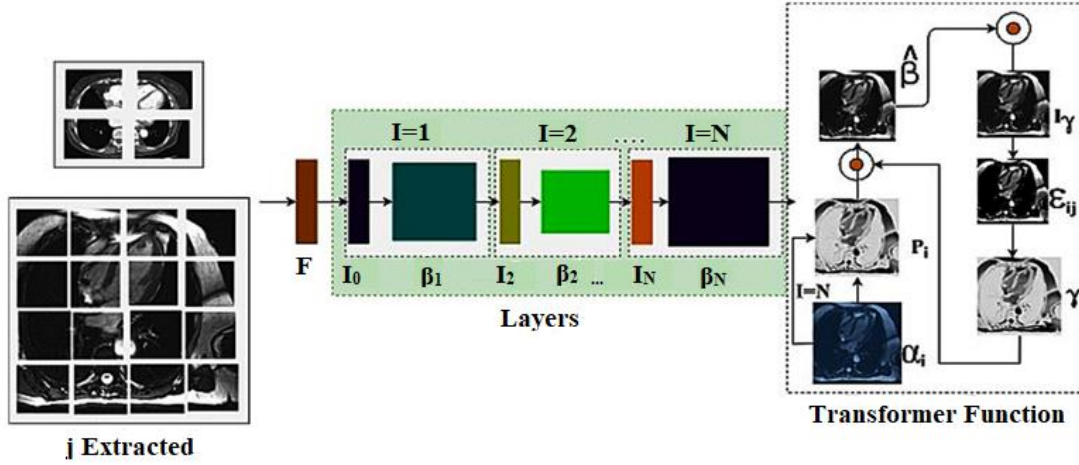


Figure 3. Segmentation process

Algorithm 1 for Segmentation

Input: γ, β

- 1: Initialize $\gamma(N) = \frac{N}{2}(\gamma * n)$
- 2: while $j = N$ do
- 3: Compute β * using Eq. (2) $\forall \beta \neq 0$
- 4: Define $\beta(j)$ for j
- 5: if $\beta(j) = \beta_\gamma(j)$
- 6: $j \in N$; check if $F \leq \beta(j)$
- 7: Perform segmentation (F, j)
- 8: Update $\hat{\beta}, \varepsilon_{ij} \forall j \in N$
- 9: else if $\beta(j) \neq \beta_\gamma(j)$ then
- 10: Perform $F \odot N$ computation
- 11: if $F \odot N \approx \frac{\gamma}{\beta}$ then
- 12: if $j = j + 1$; $\gamma(N) = \frac{n\gamma}{j}$
- 13: Update the dimension $F \forall \hat{\beta}_i$ as $F(N - \gamma \odot N)$
- 14: End if
- 15: Perform (ε_{ij}, F_n)
- 16: End while

The extracted j forms the input for the segmentation process in which $I = 1$ to $I = N$ layers are split. Based on the split, the segmentation is performed; $\hat{\beta}$ and ε_{ij} validate the transform function for training and validation. Considering the I_0 and β_N for the j , the layers are trained for the $\{F_j^i\}$ until $I = N$ is reached. This segmentation varies with F and $j \forall (2 \times 2), (4 \times$

$4), \dots (16 \times 16)$ instances. The transformer process assimilates ε_{ij} for I_γ and $\hat{\beta}_i$ provided $\bar{\alpha}_n$ satisfies $F_n(N_n \odot \beta)$ in identifying a boundary (Figure 3). Segmentation helps in accurately determining the boundaries, structures, and anomalies, easing accurate disease detection and diagnosis. The process of segmentation in the SwinTransform is explained by the following equation given above. The segmentation process is described in Algorithm 1.

Now the boundary detection procedure is performed using the SwinTransform algorithm. The boundary detection operation is established through this technique. After the data is segmented into valuable regions, the technique helps in determining and describing the boundaries that isolate these regions. It does this by assessing the pixel transitions and differences in intensity or the textural features between the adjacent segments. The process of detecting the boundaries is explained in the equation below:

$$\left. \begin{aligned}
 Z_i &= N_i(Z_{i-1}) + Z_{i-1} - 1 \\
 Z_i &= N_i([Z_0, \dots, Z_{i-1}]) \\
 \gamma &= Z^n \\
 a &= N^\gamma \\
 \beta &= N^i \\
 &\text{such that,} \\
 Z^n \cdot N^\gamma \cdot N^i &\approx 2 \\
 Z \geq 1, N \geq 1, N^i &\geq 1 \\
 Z_{ij} &= \frac{|a| + |\beta|}{|a\beta_{ij}|}
 \end{aligned} \right\} \quad (7)$$

where, Z is denoted as the boundaries detected. By precisely detecting the boundaries, the SwinTransform technique in accurately detecting the structures within the cardiac images, such as the normal functionalities of the heart and its irregularities is analyzed. This information is useful for diagnostic purposes between the cardiac structures which leads to a more understanding of the patients' cardiac health. Also based on these outcomes, the similar and disparity features are determined for the further necessities.

$$\left. \begin{aligned} V_{ij} &= \frac{\sum_{n=1} \left(\frac{-\|a_i - a_j\|^2}{2n^2 i} \right)}{\sum_{n \neq v} \left(\frac{-\|a_i - a_j\|^2}{2\gamma^2 i} \right)} \\ V_{ij} &= \frac{(V_{ji} + V_{ij})}{2n} \\ \gamma_{ij} &= \frac{(1 + \|\beta_i - \beta_j\|^2)^{-1}}{\sum_{n=1} (1 + \|\beta_n - \beta_{ij}\|^2)^{-1}} \\ Z(Q||\beta) &= \sum_i \sum_j V_{ij} \log \frac{V_{ij}}{\gamma_{ij}} \end{aligned} \right\} \quad (8)$$

where, V is denoted as the information produced by the SwinTransform procedure. Now similar features are detected from the outcome of the SwinTransform operation. This operation is engaged in determining and classifying the segments or regions that manifest similar characteristics within the cardiac MRI data. Similar features are organized for the analysis of the efficient features from the acquired MRI

input images. It enables the technique to determine the consistent frameworks across the different parts of the heart. This feature-dependent approach helps enhance the precision of disease detection and diagnosis, as it permits a better understanding of the regions with shared attributes. The process of detecting the similar features is explained in the equation given below:

$$\left. \begin{aligned} \sigma^n &= \frac{1}{V} \left(\sum_{i=1}^V a_i \right) \\ \sigma^\gamma &= \sqrt{\frac{1}{V} \sum_{i=1}^V (a_i - \sigma^n)^2} \\ \sigma &= \sqrt{\frac{\sum_{n=1} (a_{ij} * \beta_{ij})}{\sum_{n=1} (a + \beta) * \sum_{i=1} \left(\frac{a}{\beta(n)} \right)}} \\ \sigma_{ij} \left(\sum_{n=1} (a, \beta) \right) &= \frac{1}{2} \left[\sum_{n=1} \left(\frac{1}{V} (a, \beta) \right) \right] \\ \sigma(V_{ij}) &= \frac{1}{2} \sum_{n=1} \frac{a_{ij}}{\beta_{ij}(N)} \end{aligned} \right\} \quad (9)$$

where, σ is denoted as the similar features detected from the outcome of the SwinTransform. Now the disparity features are extracted. It involves determining the differences among the detected features and regions [33, 34]. These disparities may manifest as differences in textures or intensities within the segmented and classified data. The boundary detection and the disparity feature classification using the SwinTransformer are illustrated in Figure 4.

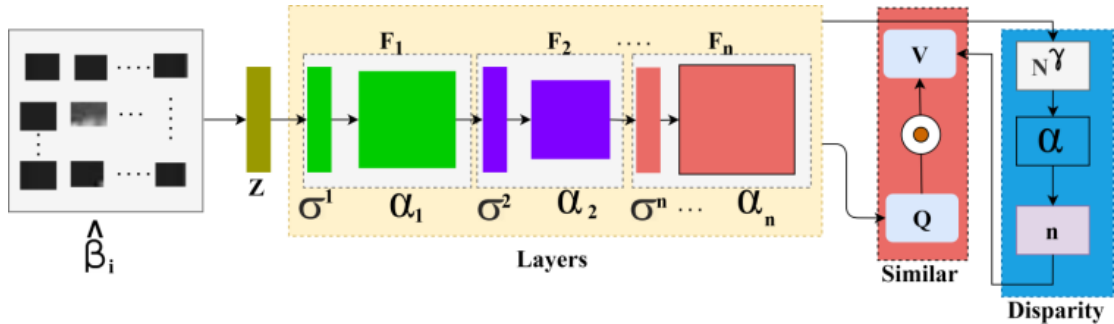


Figure 4. Boundary detection and classification

The SwinTransformer model is designed with 1 input and 1 output layers. A N consecutive layer with I_0 to I_N and β_1 to β_N with F input is sandwiched between the input and output layers. Based on the validation of $I = N$, I is incremented by 1 for I_r or ϵ_{ij} or γ reciprocating to $[\alpha_i, P_i \in \hat{\beta}]$ differences. Therefore, the initial parameters (P_i, α_i) are tuned by I and $(\beta_N - \hat{\beta})$ difference until $I = N$ condition. These N layers are dependent on the number of transformer instances required to meet the $\sum_j \forall F_n (N_n \odot \beta)$. The $\hat{\beta}_i$ inputs are used for the I process in the F_n and feature classification. The boundary detection process is performed from F_1 to F_n layers using σ^n and α_n entries matching Z . In this process, the j is required for $\sigma(V_{ij})$ estimation as in Eq. (9). The normalization using $\frac{\|\alpha_i - \alpha_j\|}{2n^2 i} \forall i \in n$ is used for feature classification across N^V for disparity. A similar feature is estimated using $V \odot Q$ assessment from n and (σ^n, α_n) outputs from Z . Therefore,

the transformer network requires F_1 to F_n for all the possible $\hat{\beta}_1$ (Figure 4). By separating these disparities, the analysis exhibits the regions that deviate from the criteria. These deviations signify efficient irregularities that need depth evaluation.

$$\left. \begin{aligned} Q &= V^Q \times a \\ \gamma &= V^\gamma \times a \\ I &= V^I \times a \\ \sum_j (Q, \gamma, I) &= \left(\frac{Q \times \gamma^T}{\sqrt{d\gamma}} \right) \times Q \\ a^t &= VN_1(a) * \beta_1 \\ a^t &= VN_2(a) * \beta_2 \\ \beta &= a^t \times a \\ Q_{ij} &= \left(\frac{\gamma_{ij} * V_{ij}}{(a, \beta)} \right) \end{aligned} \right\} \quad (10)$$

The disparity features determination operation is explained by the following equation given above. Now the coinciding features are estimated from the feature determination process outputs. This process involves determining the characteristics that coincide with each other across the different regions or segments of the acquired MRI data. These coinciding features represent similar characteristics. The evaluations of the coinciding features are an important strategy for enhancing the precision and reliability of disease detection and diagnosis in the cardiac MRI analysis, as it eases the determination of consistent cardiac features. The process of determining the coinciding features is explained in the upcoming equation:

$$\left. \begin{aligned} a^{t1} &= VN_1(a^{V-1}) + Q(a^{V-1}) \\ a^t &= VN_2(a^{t1}) + Q(a^{t1}) \\ a^{t2} &= VN_3(a^t) + Q(a^t) \\ V &= VN_4(a^{t2}) + Q(a^{t2}) \\ \frac{a^V}{a^{ij}} &= \frac{2||a \cap \beta||}{||a|| + ||\beta||} \\ &= \frac{2\gamma}{2\gamma + FV + FN} \end{aligned} \right\} \quad (11)$$

$$\left. \begin{aligned} \varphi_i &= a_i \times Q^\varphi \\ V_i &= a_i \times Q^V \\ F_i &= a_i \times Q^F \\ \beta_Q &= \beta_V \\ a_{ij} &= \sum_{n=1} \left(\frac{Q_{ij}^1}{\sqrt{V_n}} \right) \\ &= \frac{\sum_{n=1} \left(\frac{a_{ij}^1}{\sqrt{V_n}} \right)}{\sum_{j=1} \left(\frac{a_{ij}^1}{\sqrt{V_n}} \right)} \\ a_{ij}^1 &= Q_i \times V^T \end{aligned} \right\} \quad (12)$$

where, Q is denoted as the disparities in the features, φ is denoted as the coinciding features. Now the training is provided based on the coinciding features of the SwinTransform procedures. During this operation, the algorithm technique understands the determined coinciding features that denote consistent patterns within the detected MRI data. These features help as important training, enabling the process to efficacious understanding and to categorize similar patterns in MRI scan outputs. By training on coinciding features, the SwinTransform operations become more adept at determining and interpreting irregular conditions, improving accuracy and diagnostic capabilities. The process of providing the training the SwinTransform is explained in the following equation:

$$\left. \begin{aligned} AV_i &= \int_0^1 V_i(Q_i) dQ_i \\ I_oV &= \frac{a \cap \beta}{a \cup \beta} \\ V_{a\beta} &= \frac{\sum_{n=1} AV_i}{n} \\ \epsilon_{ij} &= \frac{1}{T} \\ AV_{ij} &= \int_0^1 \frac{V_i}{\gamma_i} (Q_i) * \int_0^1 Q_{ij} \\ V(Q * N) &= \frac{a \cap \beta}{a \cup \beta} * N \left(\frac{\gamma \cup \beta}{\gamma \cap \beta} \right) \end{aligned} \right\} \quad (13)$$

where, ϵ is denoted as the training provided based on the determined coinciding features. Now the independent boundary is determined based on the prior process outputs. Independent boundaries exhibit unique characteristics or differences, distinct from the coinciding features [35]. This identification helps the technique to determine the boundaries that represent the particular cardiac structures, enhancing the precision of the analysis. The process of extracting the independent boundary as per the previous process is explained by the following equation given below:

$$\left. \begin{aligned} \mu_0 &= [F_1 + V_1, F_2 + V_2 + \dots + F_n + V_n] \\ Q_i &\leftarrow \beta_{i-1}, V_i \leftarrow \beta_{i-1}, F_i \leftarrow \gamma_{i+1} \\ V_i &= \frac{(Q_i - V_i)}{\sqrt{N/N_T}} \cdot V_i \\ \beta_i &= VN[(\beta_i^*) + (\beta_{ij}^*)] \\ &\text{where } i = 1, \dots, N \\ \beta_n &= \frac{(Q_n - V_n)}{\sqrt{V/V_T}} \cdot V_n \\ \beta_{ij} &= \left(\frac{Q_{ij} \cdot V_{ij}}{\sqrt{V/V_{ij}}} \right) \end{aligned} \right\} \quad (14)$$

where, μ is represented as the independent boundary detected from the analysis process. The overall algorithm of the feature classification is presented as Algorithm 2.

Algorithm 2 for Feature Classification

Input: n, Z

- 1: $\forall n \in Z$ do {
- 2: Compute β using equation \
\characteristics identification
- 3: Define $F \odot N \forall \beta_i$
 $\in n$ //transformer initialization
- 4: compute $I = I_o * \beta$ and $\alpha_n = f_n(F^N(n_n \odot \beta_n))$
- 5: If $\{(\alpha, \beta) = 1\}$ {then
- 6: $\gamma_{ij} = \frac{|\alpha \cap \beta| + ij}{|\alpha| + |\beta|} \forall n \in N$
- 7: if $\{y_{ij} = n + 1\}$ {then //check for consecutive pixel
- 8: $\epsilon_{ij} = 1$ such that $F_n = \gamma_{ij}$
- 9: Perform $Z_i = N_i([Z_o, \dots, Z_{i-1}])$ until $F_n \neq r_{ij}$ \check{check for new segments
- 10: Repeat from step 5 until $(\alpha, \beta) \neq 1$ Repeat the I process
- 11: Update $Z(Q||\beta) \forall n \in N$
- 12: Compute σ^n and α_n for $F_i \forall i \in n$ if $(\alpha, \beta) = 1$
- 13: if $\{\sigma(V_{ij}) > 1\}$ {then
- 14: $n = n + 1; I = V^I \times \alpha; Q = V^Q \times \alpha$ \ Update the I Variables
- 15: Repeat from step 4 until $(V_{ij}) \leq 1$
- 16: Else
- 17: $\psi_i = \alpha_i * Q^\psi$ and $\beta_Q = \beta_V$
- 18: $F_n \rightarrow \alpha_i$ and $F_i \in \beta_V \forall i < n$ //classification
- 19: end if }
- 20: Update n, i, F_i
- 21: } end if }
- 22: $\gamma_{ij} = V$ } end if }
- 23: } end for

This process helps in precise analysis of the MRI-Cardiac inputs. It also helps in mitigating the issues in the MRI-cardiac analysis. The SwinTransform helps in accurate segmentation

and boundary detection operations. From that, the similar and disparity features are estimated to provide the training for it. The independent boundaries are detected which is free from flaws post the training production process.

4. EXPERIMENTAL ASSESSMENT

Table 1. Dimension representation

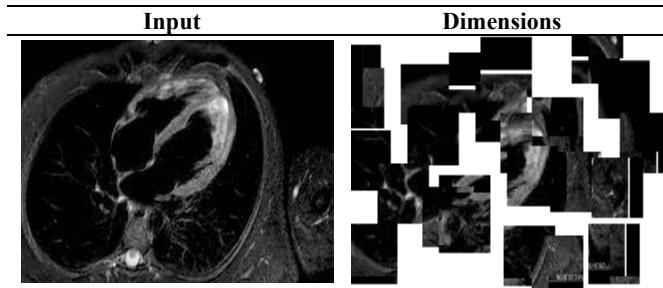


Table 2. Segmented outputs

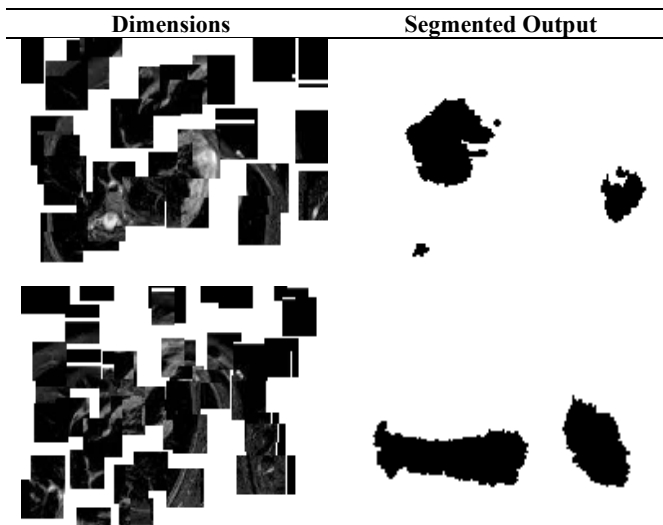
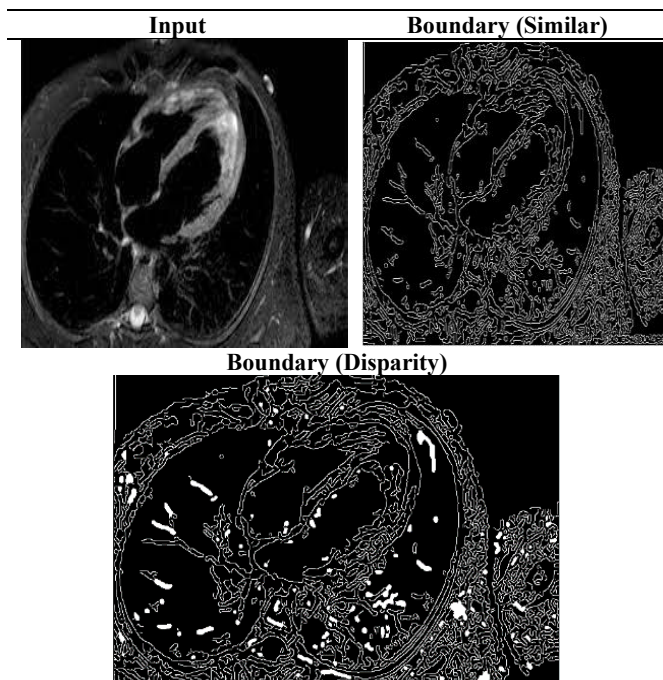
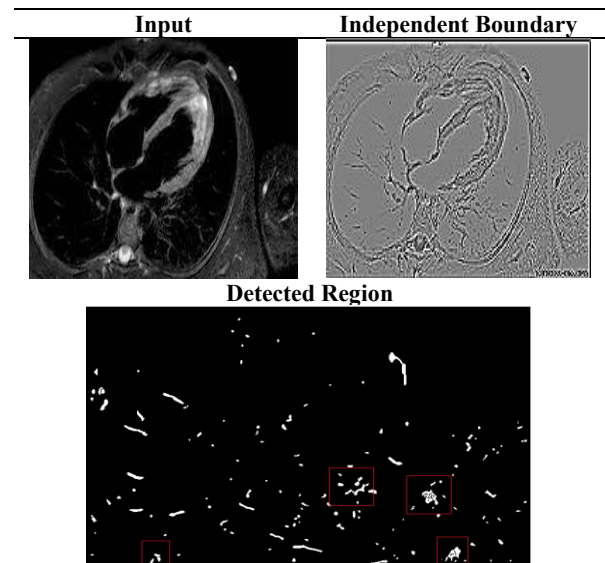


Table 3. Boundary detection



The experimental assessment is performed using MATLAB software using the inputs from the data source linked by Yoon et al. [33]. Table 1 represents the dimension representation. From this data source, the following description of the inputs is considered: the MRI cardiac inputs are acquired from 1616 patients among whom 55 are asymptotic. Table 2 illustrates the segmented outcomes. The training is pursued with the maximum inputs whereas the testing is performed using 84 MRI inputs among which 21 are disease free and 63 are diagnosed as infected. Table 3 provides the boundary detection details. The image scale varies from 10.8mm×10.8mm to 50mm×50mm in size with minimum pixel differentiation of 2×2 to 16×16. The preprocessing includes noise reduction using Gaussian filter with a histogram contrast improvement. Table 4 represents the infection detection information. The proposed method is implemented using MATLAB deployed in a computer with 8GB memory and 2.4GHz processing capacity. The maximum epochs for the network training are 800 splits into 10 recurrent iterations. Using this information, the experimental validations are performed and the results are tabulated.

Table 4. Infection detection



Apart from the above experimental analysis, the disparity with variance for the different sizes is analyzed in Table 5.

The disparity analysis is presented in the above Table 5 along with the variance estimated. The transformer function is responsible for categorizing the dimensions of similar and dissimilar features. As the size varies the various increases such that the transformer network is trained using multiple disparities. Therefore, the disparities are correlated within multiple F \odot N instances to reduce the variance to increase the accuracy. In Table 6 the precision for different layered and process outputs are tabulated.

In Table 6 the process precision for different dimensions is tabulated. The proposed transformer-based disparity detection method. Classifies different regions based on feature distribution. The distribution ensures F \odot N optimality at its highest rate through iterated training. In particular, if I's output is less than β_N is incremented to match segmentation. This process is different from the process disclosed under multiple features. The analysis of sensitivity and specificity augmenting the precision for different processes and dimensions is presented in Table 7.

Table 5. Disparity with variance for different dimensions

Type	Dimensions	Disparity	Variance	Accuracy (%)
Similar	2×2	0.16	±0.06	92.09
	4×4	0.227	±0.091	90.86
	8×8	0.293	±0.1	88.63
	16×16	0.361	±0.12	87.48
	2×2	0.069	±0.02	94.51
Heterogeneous	4×4	0.092	±0.052	93.29
	8×8	0.138	±0.068	91.77
	16×16	0.165	±0.087	91.02

Table 6. Precision outputs for I and β_N

Process	Dimension	I Output	β_N Output	Precision
Boundary	2×2	0.93	0.61	0.81
	4×4	0.925	0.654	0.854
	8×8	0.924	0.632	0.832
	16×16	0.928	0.631	0.871
	2×2	0.901	0.741	0.882
Segmentation	4×4	0.914	0.769	0.897
	8×8	0.919	0.824	0.915
	16×16	0.921	0.851	0.929
Disparity	2×2	0.901	0.897	0.925
	4×4	0.897	0.886	0.918
Detection	8×8	0.881	0.91	0.93
	16×16	0.875	0.908	0.924

Table 7. Sensitivity and specificity for different processes and dimension

Process	Dimension	False Positives	Sensitivity	Specificity
Boundary	2×2	+0.077	0.94	0.974
	4×4	+0.065	0.935	0.964
	8×8	+0.0415	0.94	0.954
	16×16	+0.0325	0.89	0.942
	2×2	+0.0254	0.94	0.854
Segmentation	4×4	+0.0189	0.98	0.841
	8×8	+0.0254	0.89	0.941
	16×16	+0.0124	0.92	0.954
Disparity	2×2	-0.04	0.87	0.921
	4×4	-0.028	0.95	0.933
Detection	8×8	-0.0147	0.926	0.872
	16×16	-0.0151	0.945	0.898

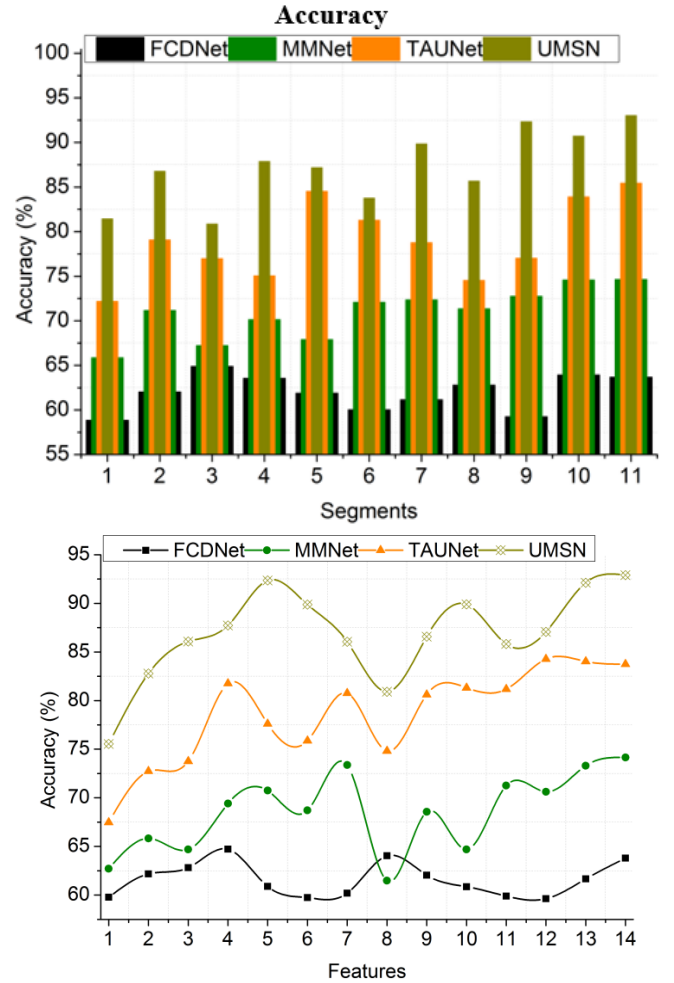
The sensitivity and specificity are illustrated for the 3 processes: boundary detection, segmentation, and disparity detection in Table 7. The consecutive $\Delta V_i \nabla \frac{V_i}{\gamma_i}$ and $\left(\frac{\alpha \cap \beta}{\gamma \cup \beta}\right)$ increases the true positives. If the false positives is increased, then $\left(\frac{\alpha \cup \beta}{\gamma \cap \beta}\right)$ is reduced confining the true negatives. Therefore, the next successive feature extraction is opted to maximize the disparity detection. The transformer model increases the chances of σ^n and α_n such that ψ_i and $F_n \rightarrow \alpha_n$ is hiked to maximize the number of f computed. Thus, if the true negative is high the consecutive N is incremented for $(I = N)$ using $V_i = (\alpha_i \times Q^v)$ for multiple f .

5. RESULTS AND DISCUSSION

Apart from the experimental analysis discussed above, this section presents the accuracy, precision, false rate, classification, and differentiation error as a comparative study. The number of segments (1 to 11) and features (1 to 14) are varied for verifying the proposed network process across each

improvement. For this comparative study, the allied methods considered are FCDNet [28], MMNet [21], and TAUNet [22]. The methods are discussed in the related works session.

The accuracy is enhanced in this method with the help of the SwinTransform method. The association of the SwinTransform method importantly improves the accuracy of the cardiac MRI analysis. This process estimates the several difficult issues that often lead to more reliable and precise results. SwinTransform pixel association and segmentation methods streamline the analysis, mitigating the risk of pixel differentiation issues. Classifying the pixels into valuable segments, permits for a more focused evaluation of the cardiac data, mitigating the irrelevant information. The SwinTransform helps determine the similar features and disparities within the acquired MRI data. It also secures the subtle frameworks and dissimilarities mitigation which help in enhancing the accuracy of the procedure. This accuracy is necessary for prior disease detection, where the small difference is indicative of the cardiac conditions. The estimation of the coinciding features and then the training on them enhances the understanding of the method, enabling it to determine consistent cardiac patterns (Figure 5).

**Figure 5.** Accuracy analysis

The precision is high in this process with the appropriate segmentation and boundary detection operation. Precision in cardiac MRI analysis is huge, as it directly affects the precision of disease detection and diagnosis. The SwinTransform algorithm pixel segmentation ensures that the cardiac images are separated into valuable segments, mitigating the irrelevant

information. This accurate segmentation allows for the main analysis, improving the accuracy of the detection and characterizing the particular regions within the heart. The feature detection precision is also enhanced during this operation which excels in detecting and extracting the characteristics with high precision. It also detects the subtle differences in textures and its intensities. The method's ability to detect the independent boundaries with accuracy is important. It secures the cardiac structures and depth irregularities are precisely defined, mitigating the risk of oversight in this MRI analysis. This operation significantly enhances the precision in identifying and classifying cardiac conditions (Figure 6).

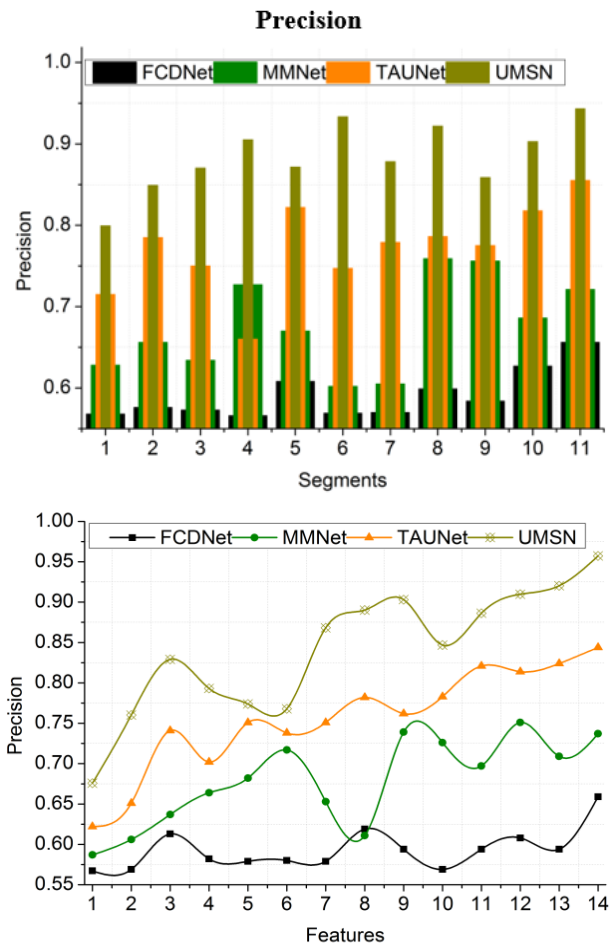


Figure 6. Precision analysis

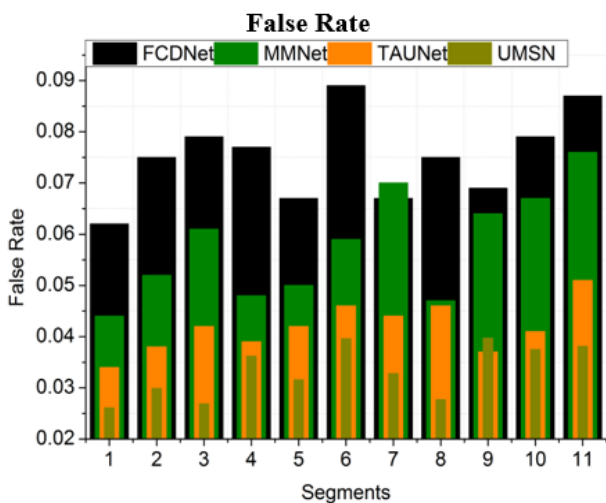


Figure 7. False rate analysis

The false rate is lesser in this process after detecting the similar and disparity features from the output of the SwinTransform operation. Exhibiting a lower false rate results in a substantial improvement in accuracy and reliability. By determining and classifying similar features within the cardiac MRI data, the system becomes perfect at determining consistent patterns. This mitigates the irregularities, which results in a significant reduction in the false positive rates. The extraction of the disparity feature is also helpful in enhancing the reduction of the inconsistencies and variations within the data, permitting the system to showcase the areas that are deviating from the measures. This results in less production of the false negatives with the enhanced MRI analysis. Training the approach on coinciding and disparity features further improves its capacity to differentiate between normal and abnormal cardiac conditions. This clarified understanding importantly mitigates the false rates where the process becomes more discerning in its assessments (Figure 7).

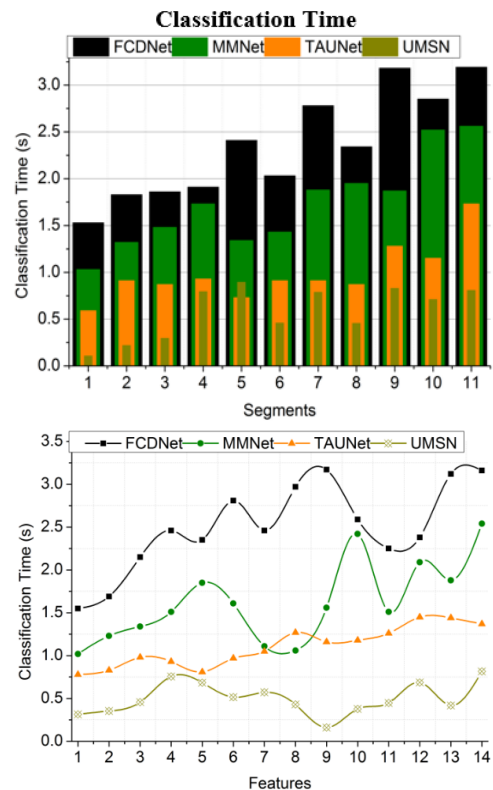


Figure 8. Classification time analysis

The time taken for the classification is less in this method using the SwinTransform algorithm. The integration of the SwinTransform in this method importantly mitigates the time needed for the classification tasks. This approach to pixel grouping and feature extraction streamlines the data analysis operation, making it more efficacious and quicker. Classifying the pixels into valuable segments and aiming at pertinent characteristics, mitigates the need for extensive resources and time-consuming manual interventions. Furthermore, the SwinTransform method's capability to determine the similarities and disparities within the data improves the categorization operation by establishing a more clarified dataset for the analysis. This efficiency permits the healthcare to obtain timely results according to the presentation of the MRI state. It helps in disease diagnosis and treatment planning for better results within a short time. The reduced classification time helps in the establishment of quicker assessments, providing improved healthcare outcomes (Figure 8).

misinterpretation. This process involves determining the characteristics that coincide with each other across the different regions or segments of the acquired MRI data. These coinciding features represent similar characteristics. During this operation, the algorithm technique understands the determined coinciding features that denote consistent patterns within the detected MRI data and thus it mitigates the differentiation errors in the operation (Figure 9). Table 8 and Table 9 presents the comparative analysis results with their discussion.

The proposed UMSN improves accuracy and precision by 9.123% and 9.96% respectively. This method reduces false rate, classification time, and differentiation error by 9.97%, 11.29%, and 10.04% respectively.

The proposed UMSN improves accuracy and precision by 9.5% and 10.53% respectively. This method reduces false rate, classification time, and differentiation error by 10.57%, 10.87%, and 10.86%, respectively.

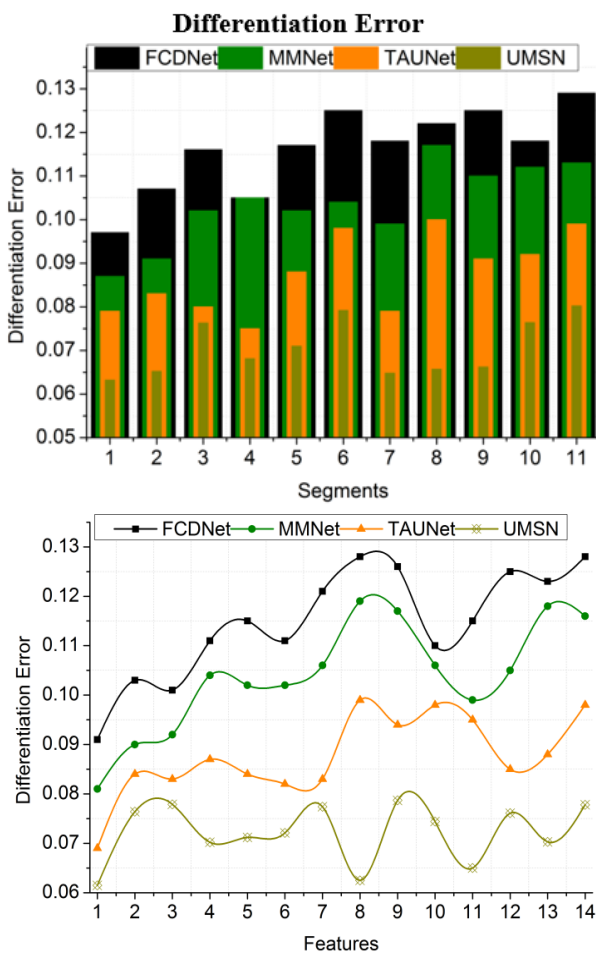


Figure 9. Differentiation error analysis

The differentiation error is lesser in this process after the precise determination of the features from the SwinTransform operation. The pixel grouping, segmentation, and feature extraction procedures enhance the overall accuracy of the cardiac MRI analysis. Classifying the pixels into meaningful segments and boundaries reduces the risk of errors arising from pixel differentiation issues. It also ensures that the data is interpreted with precision. The system's capability to determine and utilize the same and disparity features further refines its assessment of the data, mitigating the similarities

Table 8. Comparative analysis results for segments

Metrics	FCDNet	MMNet	TAUNet	UMSN
Accuracy (%)	63.67	74.63	85.44	93.005
Precision	0.656	0.721	0.855	0.9432
False Rate	0.087	0.076	0.051	0.0381
Classification Time (s)	3.19	2.56	1.73	0.806
Differentiation Error	0.129	0.113	0.099	0.0802

Table 9. Comparative analysis results for features

Metrics	FCDNet	MMNet	TAUNet	UMSN
Accuracy (%)	63.79	74.15	83.75	92.897
Precision	0.659	0.737	0.844	0.9572
False Rate	0.059	0.048	0.035	0.0262
Classification Time (s)	3.16	2.54	1.37	0.817
Differentiation Error	0.128	0.116	0.098	0.0778

6. CONCLUSION

In this article, the UMSN is designed to improve cardiac disease infection using MRI inputs. This network segregates the input for its maximum and minimum possible segments for precise feature extraction. This creative technique mitigates the inconsistency between associated and unconventional boundary segments, mitigating the fictitious feasible rate in disease detection. Moreover, the determined unit with inconsistencies between boundaries or segment pixels serves as a valuable advantage for independent training across various marked categorizations attained from the training inputs. This denotes that the operation may grasp these disparities and clarify its understanding of different cardiac conditions, thus enhancing its diagnostic precision. The proposed network improves accuracy by 9.213%, reduces false rate by 9.97%, and differentiation error by 10.04% for the varying segments.

The transformer network used in this proposed method relies on a step-by-step procedure for identifying segments for any sized inputs. The process is eventually time-consuming and computationally prolonged. Therefore, adaptable filtered transformer functions are required for reducing such complexities in the future. This leads to the design and

development of a filter transformer network with feature adaptability in the future.

REFERENCES

- [1] Bhan, A., Mangipudi, P., Goyal, A. (2023). An assessment of machine learning algorithms in diagnosing cardiovascular disease from right ventricle segmentation of cardiac magnetic resonance images. *Healthcare Analytics*, 3: 100162. <https://doi.org/10.1016/j.health.2023.100162>
- [2] Zhang, T.Y., An, D.A., Zhou, H., Ni, Z., Wang, Q., Chen, B., Wu, L.M. (2023). Fractal analysis: Left ventricular trabecular complexity cardiac MRI adds independent risks for heart failure with preserved ejection fraction in participants with end-stage renal disease. *International Journal of Cardiology*, 391: 131334. <https://doi.org/10.1016/j.ijcard.2023.131334>
- [3] Yates, T. A., Vijayakumar, R., McGilvray, M., Khiabani, A.J., Razo, N., Sinn, L., Damiano Jr, R.J. (2023). Delayed-enhancement cardiac magnetic resonance imaging detects disease progression in patients with mitral valve disease and atrial fibrillation. *JTCVS Open*, 16: 292-302. <https://doi.org/10.1016/j.xjon.2023.07.024>
- [4] Gómez, S., Romo-Bucheli, D., Martínez, F. (2022). A digital cardiac disease biomarker from a generative progressive cardiac cine-MRI representation. *Biomedical Engineering Letters*, 12(1): 75-84. <https://doi.org/10.1007/s13534-021-00212-w>
- [5] Zhang, X., Cui, C., Zhao, S., Xie, L., Tian, Y. (2023). Cardiac magnetic resonance radiomics for disease classification. *European Radiology*, 33(4): 2312-2323. <https://doi.org/10.1007/s00330-022-09236-x>
- [6] Tao, R., Zhang, S., Wang, Y., Mi, X., Ma, J., Shen, C., Zheng, G. (2021). MCG-Net: End-to-end fine-grained delineation and diagnostic classification of cardiac events from magnetocardiographs. *IEEE Journal of Biomedical and Health Informatics*, 26(3): 1057-1067. <https://doi.org/10.1109/JBHI.2021.3128169>
- [7] Ammar, A., Bouattane, O., Youssfi, M. (2021). Automatic cardiac cine MRI segmentation and heart disease classification. *Computerized Medical Imaging and Graphics*, 88: 101864. <https://doi.org/10.1016/j.compmedimag.2021.101864>
- [8] Ding, Y., Xie, W., Wong, K.K., Liao, Z. (2022). Classification of myocardial fibrosis in DE-MRI based on semi-supervised semantic segmentation and dual attention mechanism. *Computer Methods and Programs in Biomedicine*, 225: 107041. <https://doi.org/10.1016/j.cmpb.2022.107041>
- [9] Agrawal, T., Choudhary, P. (2023). Segmentation and classification on chest radiography: A systematic survey. *The Visual Computer*, 39(3): 875-913. <https://doi.org/10.1007/s00371-021-02352-7>
- [10] Ding, Y., Xie, W., Wong, K.K., Liao, Z. (2022). DE-MRI myocardial fibrosis segmentation and classification model based on multi-scale self-supervision and transformer. *Computer Methods and Programs in Biomedicine*, 226: 107049. <https://doi.org/10.1016/j.cmpb.2022.107049>
- [11] Martín-Isla, C., Campello, V.M., Izquierdo, C., Kushibar, K., Sendra-Balcells, C., Gkontra, P., Lekadir, K. (2023). Deep learning segmentation of the right ventricle in cardiac MRI: The M&Ms challenge. *IEEE Journal of Biomedical and Health Informatics*, 27(7): 3302-3313. <https://doi.org/10.1109/JBHI.2023.3267857>
- [12] Priya, S., Dhruva, D.D., Perry, S.S., Aher, P.Y., Gupta, A., Nagpal, P., Jacob, M. (2024). Optimizing deep learning for cardiac MRI segmentation: The impact of automated slice range classification. *Academic Radiology*, 31(2): 503-513. <https://doi.org/10.1016/j.acra.2023.07.008>
- [13] Hu, H., Pan, N., Liu, H., Liu, L., Yin, T., Tu, Z., Frangi, A.F. (2021). Automatic segmentation of left and right ventricles in cardiac MRI using 3D-ASM and deep learning. *Signal Processing: Image Communication*, 96: 116303. <https://doi.org/10.1016/j.image.2021.116303>
- [14] Altini, N., Prencipe, B., Cascarano, G.D., Brunetti, A., Brunetti, G., Triggiani, V., Bevilacqua, V. (2022). Liver, kidney and spleen segmentation from CT scans and MRI with deep learning: A survey. *Neurocomputing*, 490: 30-53. <https://doi.org/10.1016/j.neucom.2021.08.157>
- [15] Diao, K., Liang, H.Q., Yin, H.K., Yuan, M.J., Gu, M., Yu, P.X., He, Y. (2023). Multi-channel deep learning model-based myocardial spatial-temporal morphology feature on cardiac MRI cine images diagnoses the cause of LVH. *Insights into Imaging*, 14(1): 70. <https://doi.org/10.1186/s13244-023-01401-0>
- [16] Li, F., Li, W., Gao, X., Xiao, B. (2021). A novel framework with weighted decision map based on convolutional neural network for cardiac MR segmentation. *IEEE Journal of Biomedical and Health Informatics*, 26(5): 2228-2239. <https://doi.org/10.1109/JBHI.2021.3131758>
- [17] Xu, C., Wang, Y., Zhang, D., Han, L., Zhang, Y., Chen, J., Li, S. (2022). BMAnet: Boundary mining with adversarial learning for semi-supervised 2D myocardial infarction segmentation. *IEEE Journal of Biomedical and Health Informatics*, 27(1): 87-96. <https://doi.org/10.1109/JBHI.2022.3215536>
- [18] Wang, X., Yang, S., Fang, Y., Wei, Y., Wang, M., Zhang, J., Han, X. (2021). SK-Unet: An improved u-net model with selective kernel for the segmentation of LGE cardiac MR images. *IEEE Sensors Journal*, 21(10): 11643-11653. <https://doi.org/10.1109/JSEN.2021.3056131>
- [19] Su, C., Ma, J., Zhou, Y., Li, P., Tang, Z. (2023). Res-DUnet: A small-region attentioned model for cardiac MRI-based right ventricular segmentation. *Applied Soft Computing*, 136: 110060. <https://doi.org/10.1016/j.asoc.2023.110060>
- [20] Cui, H., Yuwen, C., Jiang, L., Xia, Y., Zhang, Y. (2021). Multiscale attention guided U-Net architecture for cardiac segmentation in short-axis MRI images. *Computer Methods and Programs in Biomedicine*, 206: 106142. <https://doi.org/10.1016/j.cmpb.2021.106142>
- [21] Wang, Z., Peng, Y., Li, D., Guo, Y., Zhang, B. (2022). MMNet: A multi-scale deep learning network for the left ventricular segmentation of cardiac MRI images. *Applied Intelligence*, 52(5): 5225-5240. <https://doi.org/10.1007/s10489-021-02720-9>
- [22] Li, D., Peng, Y., Guo, Y., Sun, J. (2022). TAUNet: A triple-attention-based multi-modality MRI fusion U-Net for cardiac pathology segmentation. *Complex & Intelligent Systems*, 8(3): 2489-2505. <https://doi.org/10.1007/s40747-022-00660-6>
- [23] Abdelrauof, D., Essam, M., Elattar, M. (2021). Light-

- weight localization and scale-independent multi-gate UNET segmentation of left and right ventricles in MRI images. *Cardiovascular Engineering and Technology*, 13: 1-14. <https://doi.org/10.1007/s13239-021-00591-2>
- [24] Joshi, A., Sharma, K.K. (2024). Dense deep transformer for medical image segmentation: DDTraMIS. *Multimedia Tools and Applications*, 83(6): 18073-18089. <https://doi.org/10.1007/s11042-023-16252-6>
- [25] Wang, Y., Zhang, Y., Xu, L., Qi, S., Yao, Y., Qian, W., Qi, L. (2023). TSP-UDANet: Two-stage progressive unsupervised domain adaptation network for automated cross-modality cardiac segmentation. *Neural Computing and Applications*, 35(30): 22189-22207. <https://doi.org/10.1007/s00521-023-08939-6>
- [26] Zou, X., Wang, Q., Luo, T. (2021). A novel approach for left ventricle segmentation in tagged MRI. *Computers and Electrical Engineering*, 95: 107416. <https://doi.org/10.1016/j.compeleceng.2021.107416>
- [27] Chen, H., Yan, S., Xie, M., Ye, Y.M., Ye, Y.G., Zhu, D., Huang, J. (2022). Fully connected network with multi-scale dilation convolution module in evaluating atrial septal defect based on MRI segmentation. *Computer Methods and Programs in Biomedicine*, 215: 106608. <https://doi.org/10.1016/j.cmpb.2021.106608>
- [28] Zhang, H., Zhang, W., Shen, W., Li, N., Chen, Y., Li, S., Wang, Y. (2021). Automatic segmentation of the cardiac MR images based on nested fully convolutional dense network with dilated convolution. *Biomedical Signal Processing and Control*, 68: 102684. <https://doi.org/10.1016/j.bspc.2021.102684>
- [29] Hu, H., Pan, N., Frangi, A.F. (2023). Fully Automatic initialization and segmentation of left and right ventricles for large-scale cardiac MRI using a deeply supervised network and 3D-ASM. *Computer Methods and Programs in Biomedicine*, 240: 107679. <https://doi.org/10.1016/j.cmpb.2023.107679>
- [30] Yan, Z., Su, Y., Sun, H., Yu, H., Ma, W., Chi, H., Chang, Q. (2022). SegNet-based left ventricular MRI segmentation for the diagnosis of cardiac hypertrophy and myocardial infarction. *Computer Methods and Programs in Biomedicine*, 227: 107197. <https://doi.org/10.1016/j.cmpb.2022.107197>
- [31] Singh, K.R., Sharma, A., Singh, G.K. (2023). Attention-guided residual W-Net for supervised cardiac magnetic resonance imaging segmentation. *Biomedical Signal Processing and Control*, 86: 105177. <https://doi.org/10.1016/j.bspc.2023.105177>
- [32] Suganyadevi, S., Seethalakshmi, V., Anandan, P., Renu, K. (2023). Integrated model for COVID 19 disease diagnosis using deep learning approach. In *2023 2nd International Conference on Edge Computing and Applications (ICECAA)*, Namakkal, India, pp. 576-582. <https://doi.org/10.1109/ICECAA58104.2023.10212181>
- [33] Yoon, S., Nakamori, S., Amyar, A., Assana, S., Cirillo, J., Morales, M.A., Nezafat, R. (2023). Accelerated cardiac MRI cine with use of resolution enhancement generative adversarial inline neural network. *Radiology*, 307(5): e222878. <https://doi.org/10.1148/radiol.222878>
- [34] Suganyadevi, S., Seethalakshmi, V. (2024). Deep recurrent learning based qualified sequence segment analytical model (QS2AM) for infectious disease detection using CT images. *Evolving Systems*, 15(2): 505-521. <https://doi.org/10.1007/s12530-023-09554-5>
- [35] Suganyadevi, S., Rajasekaran, A.S., Satheesh, N.P., Suganthi, R., Naveenkumar, R. (2023). Alzheimer's disease diagnosis using deep learning approach. In *2023 Second International Conference on Electronics and Renewable Systems (ICEARS)*, Tuticorin, India, pp. 1205-1209. <https://doi.org/10.1109/ICEARS56392.2023.10085017>